AIAA JOURNAL
Vol. 36, No. 1, January 1998

Improved Low-Reynolds-Number k–$\tilde{\varepsilon}$ Model Based on Direct Numerical Simulation Data

C. B. Hwang* and C. A. Lin†
National Tsing Hua University, Hsinchu, Taiwan 30043, Republic of China

An improved low-Reynolds-number k–$\tilde{\varepsilon}$ turbulence model is proposed. The model is designed not only to conform with the near-wall characteristics obtained with direct numerical simulation data but also to possess the correct asymptotic behavior in the vicinity of the wall. The key features of this model are the adoption of the Taylor microscale in the damping function and the inclusion of the pressure diffusion terms in the k and $\tilde{\varepsilon}$ equations. Further applications of the present model to a two-dimensional backward-facing step flow indicate that the present model reproduces correctly the skin-friction and near-wall heat transfer coefficients.

I. Introduction

IT is a common practice to apply the logarithmic law of the wall in computing wall-bounded flow fields, due to its simplicity and lower demand on fine-grid distributions to resolve the rapid variation of the flow properties in the near-wall region. Launder[1] indicated, however, that in many cases applying the low-Reynolds-number turbulence models in the near-wall region caused a marked improvement over the wall function approach in predicting the local heat transfer coefficients. This improvement is rooted on the sufficiently resolved turbulence transport processes and consequently the heat transfer characteristics in the vicinity of the wall.

In the past, various forms of low-Reynolds-number k–ε turbulence models have been proposed,[2–5] but due to the lack of detailed and reliable measurements of the near-wall turbulence structure, the forms of the model were based on ad hoc adjustments of the model constants and damping functions to reproduce the flowfields. The arrival of direct numerical simulation (DNS)[6,7] shed some light on the detailed flow structure in the near-wall region, and the detailed energy budgets derived from the DNS data provide a route toward the modeling of wall turbulence. Further, the asymptotic analysis, which is supported by DNS data, provides a powerful tool for analyzing the forms of the models. However, few of the many proposed models completely satisfy the asymptotic limit and the DNS data.

In this paper, an $\tilde{\varepsilon}$ $(=\varepsilon - 2\nu[\partial\sqrt{k}/\partial y]^2)$ equation is adopted instead of the ε equation. Key features of the k–$\tilde{\varepsilon}$ model are the adoption of the Taylor microscale in the damping functions and the inclusion of the pressure diffusion terms in both the k and $\tilde{\varepsilon}$ equations. The predictive performance of the model is assessed by comparisons with DNS data for fully developed channel flows and measurements of the two-dimensional backward-facing step flow.

II. Governing Equations

The Reynolds-averaged continuity, Navier–Stokes, and temperature equations can be written as

$$\frac{\partial U_j}{\partial x_j} = 0 \tag{1}$$

$$\frac{\partial U_j U_i}{\partial x_j} = -\frac{1}{\rho}\frac{\partial P}{\partial x_i} + \frac{\partial}{\partial x_j}\left[\nu\left(\frac{\partial U_i}{\partial x_j} + \frac{\partial U_j}{\partial x_i}\right) - \overline{u_i u_j}\right] \tag{2}$$

$$\frac{\partial U_j T}{\partial x_j} = \frac{\partial}{\partial x_j}\left(\frac{\nu}{\sigma}\frac{\partial T}{\partial x_j} - \overline{u_j\theta}\right) \tag{3}$$

where ν and σ are kinematic viscosity and Prandtl numbers, respectively.

Within the framework of eddy viscosity and adopting the Boussinesq approximation, the Reynolds stress and heat flux are approximated as

$$-\overline{u_i u_j} = \nu_t\left(\frac{\partial U_i}{\partial x_j} + \frac{\partial U_j}{\partial x_i}\right) - \frac{2}{3}\delta_{ij}k \tag{4}$$

$$-\overline{u_j\theta} = \frac{\nu_t}{\sigma_t}\frac{\partial T}{\partial x_j} \tag{5}$$

where ν_t and σ_t are turbulent kinematic viscosity and Prandtl numbers, respectively. The value of σ_t is chosen to be 0.9 (Ref. 2).

In the present applications, the turbulence model adopted is the k–$\tilde{\varepsilon}$ model.[2] When applying the model toward the wall, the contribution of molecular viscosity on the shear stress increases, and the standard high-Reynolds-number turbulence must be modified to account for the diminishing effect of the near-wall turbulence levels. The construction of the low-Reynolds-number model is the focus of the next section.

III. Near-Wall Modeling

A. Turbulent Kinetic Energy Equation

To model the k equation in the low-Reynolds-number region, it would be beneficial to examine first the exact form of the transport equation, which can be expressed as[8]

$$\frac{\partial U_j k}{\partial x_j} = \underbrace{\frac{\partial}{\partial x_j}\left(\nu\frac{\partial k}{\partial x_j}\right)}_{\mathcal{D}_k} \underbrace{-\frac{\partial}{\partial x_j}\left(\frac{1}{2}\overline{u_i u_i u_j}\right)}_{\mathcal{T}_k} \underbrace{-\frac{1}{\rho}\frac{\partial}{\partial x_j}(\overline{pu_j})}_{\Pi_k}$$

$$\underbrace{-\overline{u_i u_j}\frac{\partial U_i}{\partial x_j}}_{\mathcal{P}_k} \underbrace{-\nu\overline{\frac{\partial u_i}{\partial x_j}\frac{\partial u_i}{\partial x_j}}}_{\varepsilon} \tag{6}$$

where $\mathcal{D}_k$, $\mathcal{T}_k$, Π_k, $\mathcal{P}_k$, and ε are the laminar diffusion, turbulent diffusion, pressure diffusion, turbulent production, and turbulent dissipation rate, respectively.

Before proceeding to the analysis of the near-wall asymptotic behavior of the different terms in the equation, it would be useful to examine the variations of the instantaneous velocity components with the distance from the wall y. Following Launder,[8] this can be expressed as

$$u = b_1 y + c_1 y^2 + d_1 y^3 + \cdots \tag{7}$$

$$v = c_2 y^2 + d_2 y^3 + \cdots \tag{8}$$

$$w = b_3 y + c_3 y^2 + d_3 y^3 + \cdots \tag{9}$$

Received Oct. 26, 1996; presented as Paper 97-0720 at the AIAA 35th Aerospace Sciences Meeting, Reno, NV, Jan. 6–10, 1997; revision received July 18, 1997; accepted for publication Sept. 6, 1997.

*Graduate Student, Department of Power Mechanical Engineering.
†Associate Professor, Department of Power Mechanical Engineering. Member AIAA.

where the coefficients b_i, c_i, and d_i are functions of time whose mean value must be zero because $\overline{u_i} = 0$. Therefore, the Reynolds stresses can be expressed as

$$\overline{u^2} = \overline{b_1^2}y^2 + 2\overline{b_1 c_1}y^3 + \left(\overline{c_1^2} + 2\overline{b_1 d_1}\right)y^4 + \cdots \tag{10}$$

$$\overline{v^2} = \overline{c_2^2}y^4 + \cdots \tag{11}$$

$$\overline{w^2} = \overline{b_3^2}y^2 + 2\overline{b_3 c_3}y^3 + \left(\overline{c_3^2} + 2\overline{b_3 d_3}\right)y^4 + \cdots \tag{12}$$

$$\overline{uv} = \overline{b_1 c_2}y^3 + (\overline{c_1 c_2} + \overline{b_1 d_2})y^4 + \cdots \tag{13}$$

and $k = \overline{u_i u_i}/2$ and $\varepsilon = \nu[\overline{(\partial u_i/\partial x_j)(\partial u_i/\partial x_j)}]$ are

$$k = \tfrac{1}{2}\left(\overline{b_1^2} + \overline{b_3^2}\right)y^2 + (\overline{b_1 c_1} + \overline{b_3 c_3})y^3 + \cdots$$
$$= \tfrac{1}{2}by^2 + cy^3 + dy^4 + \cdots \tag{14}$$

$$\varepsilon = \nu b + 4\nu c y + d_\varepsilon y^2 + \cdots \tag{15}$$

By inserting the newly derived y-dependent turbulent quantities into the k equation, it can be shown that, in the near-wall region, convection, turbulent diffusion, and production terms go to zero very rapidly. Therefore, the asymptotic behavior of the remaining terms, laminar diffusion $\mathcal{D}_k$, pressure diffusion Π_k, and dissipation rate ε, can be derived as[8]

$$\mathcal{D}_k = \nu b + 6\nu c y + \cdots \tag{16}$$

$$\Pi_k = -2\nu c y + \cdots \tag{17}$$

$$-\varepsilon = -\nu b - 4\nu c y + \cdots \tag{18}$$

From order of magnitude analysis, only these terms prevail in the near-wall region, and the inclusion of the pressure diffusion term compensates the unbalanced first-order term.[9] It was the common belief that the dissipation rate reached its maximum value somewhere inside the viscous sublayer.[10] However, DNS data show a negative value of c (Ref. 6), $\partial\varepsilon/\partial y = 4\nu c < 0$ at the wall, and this indicates that the maximum value of dissipation rate should be located at the wall itself. These, as argued by Kawamura,[9] necessitate the inclusion of Π_k in the k equation, especially in the near-wall region. DNS indicates the influences of the pressure diffusion term decay rapidly away from the wall; therefore Π_k is modeled as[9]

$$\Pi_k = -\frac{1}{2}\nu\frac{\partial}{\partial y}\left[\frac{k}{\varepsilon}\frac{\partial\hat{\varepsilon}}{\partial y}\right] = -2\nu c y + \cdots \tag{19}$$

where $\hat{\varepsilon}$ is defined as

$$\hat{\varepsilon} = 2\nu\left(\frac{\partial\sqrt{k}}{\partial y}\right)^2 = \nu b + 4\nu c y + d_{\hat{\varepsilon}} y^2 + \cdots \tag{20}$$

It is also apparent that $\hat{\varepsilon}_w$ stands for the nonzero value of dissipation rate at the wall ε_w. Because $\hat{\varepsilon}$ approaches 0 at about $y^+ > 15$, this formulation makes the influence of Π_k confined to the wall region.

B. Turbulent Dissipation Rate Equation

Now attention is directed to the modeling of turbulent dissipation rate ε. There are currently two directions in solving the dissipation rate equation. The first one is the solution of the ε equation. The second approach is the decomposition of the dissipation rate into two parts, i.e., $\varepsilon = \tilde{\varepsilon} + \hat{\varepsilon}$, and adopting $\tilde{\varepsilon}$ as the dependent variable. Therefore, $\tilde{\varepsilon}$ is defined as the difference of $\varepsilon\,[= \nu\overline{(\partial u_i/\partial x_j)(\partial u_i/\partial x_j)}]$ and $\hat{\varepsilon}\,[= 2\nu(\partial\sqrt{k}/\partial y)^2]$. The asymptotic behavior of $\tilde{\varepsilon}$ is

$$\tilde{\varepsilon} = \varepsilon - \hat{\varepsilon} = (d_\varepsilon - d_{\hat{\varepsilon}})y^2 + \cdots \tag{21}$$

As indicated earlier, $\hat{\varepsilon}_w$ stands for the nonzero value of dissipation rate at the wall ε_w. Therefore, the advantage of this approach is that $\tilde{\varepsilon}$ reaches zero at the wall and $\tilde{\varepsilon}$ equals to ε at about $y^+ > 15$ where $\hat{\varepsilon}$ approaches 0.

The commonly adopted form of the $\tilde{\varepsilon}$ equation can be expressed as[3]

$$\frac{\partial U_j\tilde{\varepsilon}}{\partial x_j} = \frac{\partial}{\partial x_j}\left(\nu\frac{\partial\tilde{\varepsilon}}{\partial x_j}\right) + \frac{\partial}{\partial x_j}\left(\frac{\nu_t}{\sigma_\varepsilon}\frac{\partial\tilde{\varepsilon}}{\partial x_j}\right)$$
$$+ C_{\varepsilon 1}f_1\mathcal{P}_k\frac{\tilde{\varepsilon}}{k} - C_{\varepsilon 2}f_2\frac{\tilde{\varepsilon}^2}{k} + \cdots \tag{22}$$

In the vicinity of the wall, convection, turbulent diffusion, and production go to zero very rapidly, and the asymptotic behaviors of the remaining terms are

$$\frac{\partial}{\partial y}\left[\nu\frac{\partial\tilde{\varepsilon}}{\partial y}\right] = 2\nu(d_\varepsilon - d_{\hat{\varepsilon}}) + \cdots \tag{23}$$

$$C_{\varepsilon 2}f_2\frac{\tilde{\varepsilon}^2}{k} = C_{\varepsilon 2}f_2\frac{\left[(d_\varepsilon - d_{\hat{\varepsilon}})y^2 + \cdots\right]^2}{\frac{1}{2}by^2 + cy^3 + dy^4 + \cdots} \to 0 \tag{24}$$

This necessitates the inclusion of the pressure diffusion to balance the equation, and the form adopted is

$$\Pi_{\hat{\varepsilon}} = -\nu\frac{\partial}{\partial y}\left[\frac{\tilde{\varepsilon}}{k}\frac{\partial k}{\partial y}\right] = -2\nu(d_\varepsilon - d_{\hat{\varepsilon}}) + \cdots \tag{25}$$

This form was first suggested by Launder,[8] albeit in the ε equation. The idea of the inclusion of $\Pi_{\hat{\varepsilon}}$ to balance the molecular diffusion at the wall was also adopted by Chien[4] and Kawamura,[9] though with different formulations. However, only the present formulation mimics the diffusive nature of the pressure diffusion term. Furthermore, the proposed modeled $\Pi_{\hat{\varepsilon}}$ also generates the extra source for ε in the buffer zone, completely replacing the commonly adopted function, $\nu\nu_t(\partial^2 U_i/\partial x_j\partial x_k)(\partial^2 U_i/\partial x_j\partial x_k)$.

C. Proposed Model

The proposed forms of the turbulent kinetic and dissipation rate equations are

$$\frac{\partial U_j k}{\partial x_j} = \frac{\partial}{\partial x_j}\left[\left(\nu + \frac{\nu_t}{\sigma_k}\right)\frac{\partial k}{\partial x_j}\right] - \frac{1}{2}\frac{\partial}{\partial x_j}\left(\nu\frac{k}{\varepsilon}\frac{\partial\hat{\varepsilon}}{\partial x_j}\right)$$
$$- \overline{u_i u_j}\frac{\partial U_i}{\partial x_j} - (\tilde{\varepsilon} + \hat{\varepsilon}) \tag{26}$$

$$\frac{\partial U_j\tilde{\varepsilon}}{\partial x_j} = \frac{\partial}{\partial x_j}\left[\left(\nu + \frac{\nu_t}{\sigma_\varepsilon}\right)\frac{\partial\tilde{\varepsilon}}{\partial x_j}\right] - \frac{\partial}{\partial x_j}\left(\nu\frac{\tilde{\varepsilon}}{k}\frac{\partial k}{\partial x_j}\right)$$
$$- C_{\varepsilon 1}f_1\frac{\tilde{\varepsilon}}{k}\overline{u_i u_j}\frac{\partial U_i}{\partial x_j} - C_{\varepsilon 2}f_2\frac{\tilde{\varepsilon}^2}{k} \tag{27}$$

where

$$\nu_t = (k^2/\tilde{\varepsilon})C_\mu f_\mu(y_\lambda) \tag{28}$$

The coefficients and the damping functions are

$$C_\mu = 0.09, \qquad C_{\varepsilon 1} = 1.44, \qquad C_{\varepsilon 2} = 1.92$$

$$f_\mu = 1 - \exp\left(-0.01y_\lambda - 0.008y_\lambda^3\right)$$

$$\sigma_k = 1.4 - 1.1\exp[-(y_\lambda/10)]$$

$$\sigma_\varepsilon = 1.3 - 1.0\exp[-(y_\lambda/10)]$$

$$f_1 = 1, \qquad f_2 = 1$$

where $y_\lambda = y/\sqrt{(\nu k/\tilde{\varepsilon})}$ and $\sqrt{(\nu k/\tilde{\varepsilon})}$ is the Taylor microscale. The adopted form of f_μ reproduces correctly the asymptotic limit, i.e., $f_\mu \propto y$ and hence $\overline{uv} \propto y^3$ toward the wall. The adoption of y_λ avoids the obvious defect, i.e., the singularity occurring at the reattaching point by adopting $y^+ = u_\tau y/\nu$. Practically, $y_\lambda = y/\sqrt{(\nu k/\tilde{\varepsilon})} = y/[(k^{3/2}/\tilde{\varepsilon})/R_t^{1/2}]$ could serve as a length-scale damping factor when approaching the wall, and accounts for the wall-proximity size of eddies that are of the order of the wall distance y.

The constants in the model are chosen so that the present model retains its high-Reynolds-numberform away from solid boundaries. The asymptotic values of turbulent Prandtl number σ_k and σ_ε are adopted as 0.3 to obtain sufficient diffusion in the vicinity of the wall. In the core region of the flow, $\sigma_k > \sigma_\varepsilon$ is chosen to eliminate the common drawback where the turbulent diffusion of k overwhelms that of ε (Refs. 11 and 12). In the preliminary studies, the function $f_2 = 1 - 0.22\exp[-(R_t/6)^2]$ was chosen to match the final period of decay of isotropic turbulence, which originates from the work of Hanjalic and Launder.[12] However, the predicted results differ marginally with those adopting $f_2 = 1$.

Here, the performances of the k–$\tilde{\varepsilon}$ models proposed by Launder and Sharma[3] (referred to as LS) and Chien[4] (referred as CH), which were rated best in the reviews by Patel et al.[13] and Savill,[14] are to be contrasted with the present model.

IV. Numerical Procedure

The present numerical procedure[15] solves discretized versions of all equations over a staggered finite volume arrangement. The principle of mass-flux continuity is imposed indirectly via the solution of pressure-correction equations according to the SIMPLE algorithm.[16] The flow-property values at volume faces contained in the convective fluxes, which arise from the finite volume integration process, are approximated by the quadratic upstream-weighted interpolation scheme (QUICK).[17]

It was found that the employment of the third-order approximation of the surface derivatives arising from the viscous and pressure diffusion processes is essential in reproducing the correct flow near-wall asymptotic behavior, by ensuring that the derivative is evaluated right at the surface.

The computed solution is assumed to have converged to its steady state when the magnitude of the absolute residual sources of mass and momentum, normalized by the respective inlet fluxes, falls below 0.01%.

V. Results and Discussions

A. Fully Developed Channel Flows

The performance of the proposed model is first contrasted with the DNS data of fully developed channel flows,[6] with Reynolds number being $Re_\tau = 3.95 \times 10^2$ and 1.80×10^2, respectively. The $Re_\tau = 3.95 \times 10^2$ case was used to calibrate the present model coefficients, f_μ, σ_k, and σ_ε. Grid densities of sizes 60, 100, and 160 in the direction normal to the wall were used to check the grid independence. Preliminary results indicated that the three meshes produced nearly identical results; therefore, the 60 grid was used for all subsequent calculations. To ensure the resolution of the viscous sublayer, the first grid node near the wall was placed at $y^+ \approx 0.1$.

The asymptotic behaviors of $k^+(= k/U_\tau^2)$, $-\overline{uv}^+(= -\overline{uv}/U_\tau^2)$, and $\tilde{\varepsilon}^+(= \tilde{\varepsilon}\nu/U_\tau^4)$ in the near-wall region with $Re_\tau = 3.95 \times 10^2$, are shown in Figs. 1–3. The term U_τ is the friction velocity and is defined as $U_\tau = \sqrt{(\tau_w/\rho)}$. The results indicate that the present model predicts the correct limiting behaviors, and the rest of the two models do not satisfy the quadratic or cubic variation of the turbulent quantities, i.e., $k \sim y^2$, $-\overline{uv} \sim y^3$, and $\tilde{\varepsilon} \sim y^2$. Similarly, the f_μ, shown in Fig. 4, is also well represented by the present model in comparison with the DNS[18] and Patel's data.[13] In the region very close to the wall, f_μ increases proportional to y to ensure the correct cubic power-law behavior of the Reynolds stress, i.e., $-\overline{uv} \propto y^3$. While in the elevated Reynolds number region, the value of f_μ approaches 1, to ensure the model being compatible to the standard high-Reynolds k–ε turbulence model. Note, however, that the DNS data were evaluated using the formulation $\nu_t = C_\mu f_\mu k^2/\varepsilon$, in which case f_μ varies inversely with y, i.e., $f_\mu \sim 1/y$. The present model, on the other hand, adopts the form $\nu_t = C_\mu f_\mu k^2/\tilde{\varepsilon}$, and in the near-wall region f_μ increases proportionally to y. Therefore, the present model should match the DNS data in the regions $y^+ > 15$, where ε and $\tilde{\varepsilon}$ are equal.

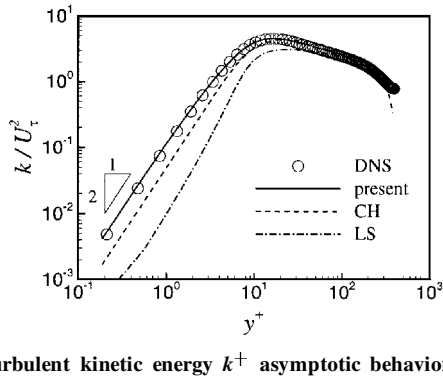

Fig. 1 Turbulent kinetic energy k^+ asymptotic behaviors: Re_τ = 3.95×10^2.

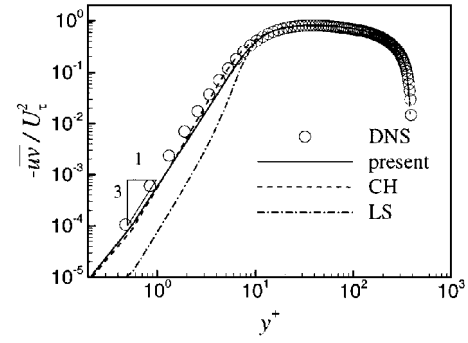

Fig. 2 Shear stress $-\overline{uv}^+$ asymptotic behaviors: $Re_\tau = 3.95 \times 10^2$.

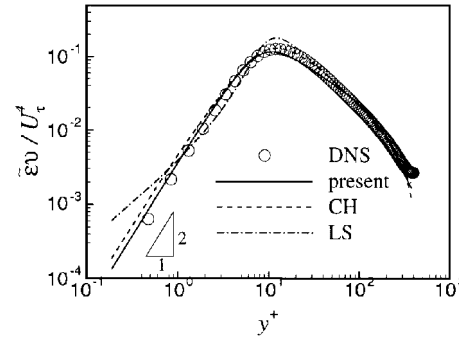

Fig. 3 Turbulent dissipation rate $\tilde{\varepsilon}^+$ asymptotic behaviors: Re_τ = 3.95×10^2.

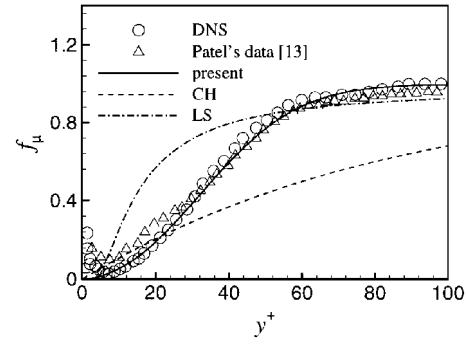

Fig. 4 Damping function f_μ distributions: $Re_\tau = 3.95 \times 10^2$.

Further examination of the performance of the models can be directed to the k^+ distributions of the $Re_\tau = 3.95 \times 10^2$ and 1.80×10^2 cases, shown in Figs. 5 and 6 for the near-wall region. Although the Launder and Sharma model underpredicted the peak value, the best result is predicted by the proposed model. The effect of the inclusion of pressure diffusion terms, as indicated earlier, is best exemplified by observing the ε^+ distributions in the near-wall region, shown in Figs. 7 and 8. The present model shows the correct level of ε with the maximum located at the wall, and in strong contrast, the CH and LS models indicate misplaced local maxima. The elevated level of the dissipation rate, due to the increase of Reynolds number, is also captured by the present model.

The overall performance of the model is evaluated by examining the predicted turbulence kinetic energy budget, shown in Figs. 9 and

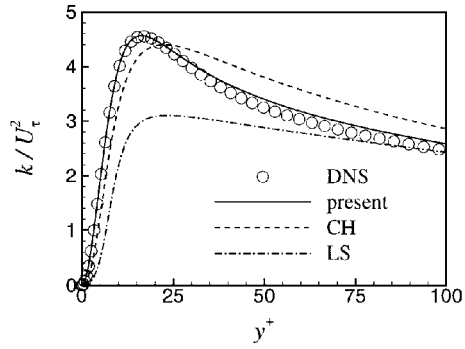

Fig. 5 Turbulent kinetic energy k^+ distributions: $Re_\tau = 3.95 \times 10^2$.

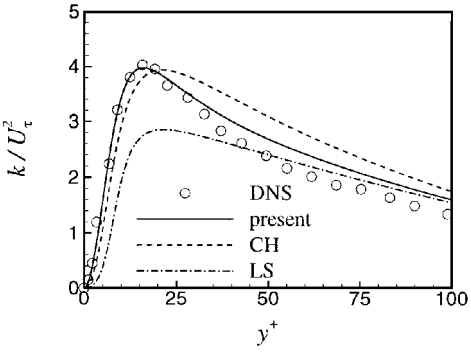

Fig. 6 Turbulent kinetic energy k^+ distributions: $Re_\tau = 1.80 \times 10^2$.

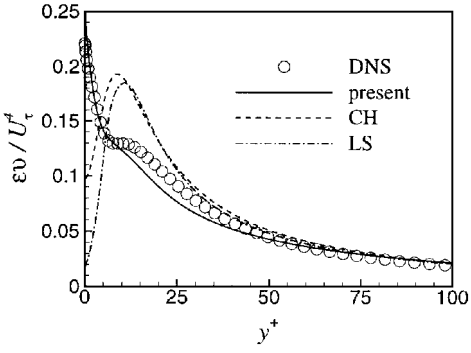

Fig. 7 Turbulent dissipation rate ε^+ distributions: $Re_\tau = 3.95 \times 10^2$.

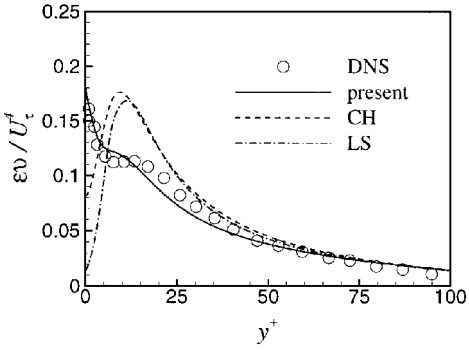

Fig. 8 Turbulent dissipation rate ε^+ distributions: $Re_\tau = 1.80 \times 10^2$.

10, for the $Re_\tau = 3.95 \times 10^2$ and 1.80×10^2 cases, respectively. By contrasting with DNS data, the quality of the model predictions can be further ascertained. The k-budget is in general dominated by production and dissipation processes away from the wall. In the vicinity of the wall, the dissipation rate balances the viscous diffusion process.

B. Turbulent Plane Couette–Poiseuille Flow

The performance of the proposed model is further contrasted with the DNS data of the fully developed plane Couette–Poiseuille flow.[19] The schematic picture of the flow is shown in Fig. 11, where the top wall is at rest and the bottom wall is moving at a constant speed U_w. The Reynolds number based on the channel half-width δ and the bottom wall velocity is 1.8×10^3. Grid densities of sizes 60 and 100 in the direction normal to the wall were used to check the grid independence, and the 60 grid was found enough. The first grid node near the wall was placed at $y^+ \approx 0.1$ to ensure the adequate resolution of the viscous sublayer.

The influence of the moving wall on the flow can be seen by the asymmetric axial velocity distribution across the channel, shown in Fig. 12, where the location of the maximum axial velocity is observed to shift toward the moving wall. The velocity distribution at the top wall side is similar to that obtained from the fully developed channel flow. However, a markedly different profile is observed at the moving bottom wall region, shown in Fig. 13, and the velocity distribution is well predicted by the proposed model. Note that $U_{\tau t}$ and $U_{\tau b}$ are the friction velocity at the top and bottom walls, respectively.

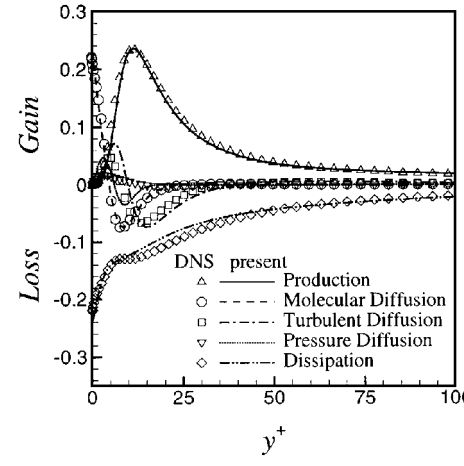

Fig. 9 Turbulent kinetic energy budget distributions: $Re_\tau = 3.95 \times 10^2$.

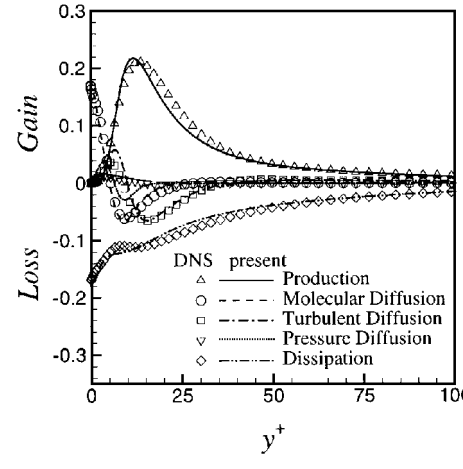

Fig. 10 Turbulent kinetic energy budget distributions: $Re_\tau = 1.80 \times 10^2$.

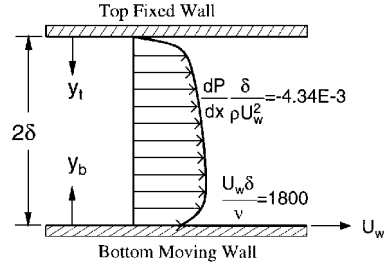

Fig. 11 Geometry of turbulent plane Couette–Poiseuille flow.

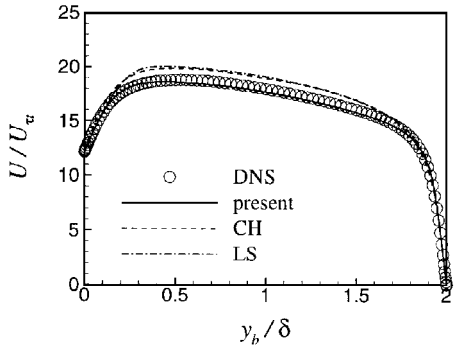

Fig. 12 Mean velocity profiles; $U_{\tau t}$ denotes the friction velocity at the top wall.

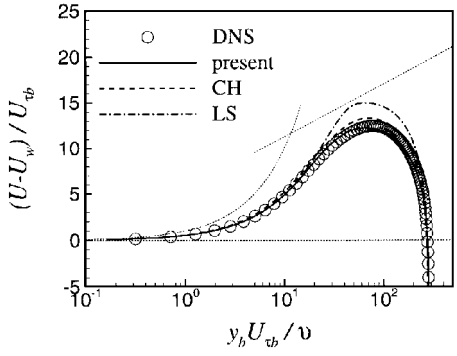

Fig. 13 Mean velocity plotted from the bottom wall; $U_{\tau b}$ denotes the friction velocity at the bottom wall.

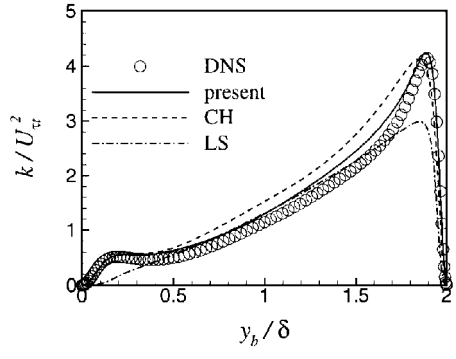

Fig. 14 Turbulent kinetic energy profiles.

Because of the reduction of the shear stress at the moving wall, the turbulent kinetic energy level adjacent to the bottom wall is severely damped, as can be seen in Fig. 14, compared with the k level at the top wall side. The performances of the models near the stationary side are similar to those observed in the previous section. However, at the bottom wall, the k level predicted by the LS model decays monotonically, which is inconsistent with the DNS data distribution.

As observed in the previous section, the local maximum of ε is located at the wall near the stationary side. At the region $y_b^+ (= y_b U_{\tau b}/\nu) < 20$ on the moving wall side, the local maximum of ε is again found at the wall, shown in Fig. 15, and this is reproduced correctly by the proposed model. The CH prediction shows a rise to its local maximum and then decays monotonically toward the wall. However, the LS prediction decays monotonically toward the wall at $y_b^+ < 20$. Finally, the performance of the proposed model can be ascertained by observing the turbulent kinetic energy budget near the moving wall, shown in Fig. 16.

C. Turbulent Flow over a Backward-Facing Step

To explore the model's performance in complex environments, the model is further applied to simulate flow at a backward-facing step.[20] Measurements of the flow quantities as well as wall heat transfer characteristics are available to further evaluate the model's performance. The geometry of the backward-facing step is shown in Fig. 17. The Reynolds number of the flow, based on the step height,

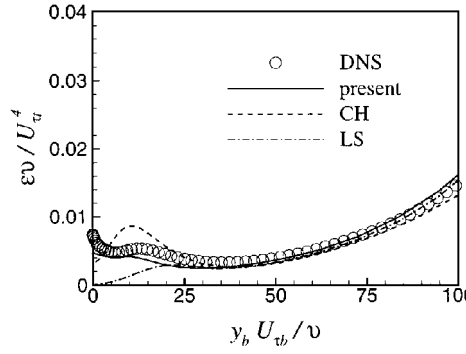

Fig. 15 ε^+ distributions: bottom wall.

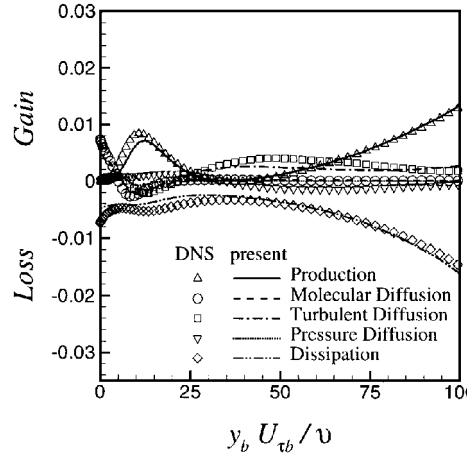

Fig. 16 Turbulent kinetic energy budget: bottom wall.

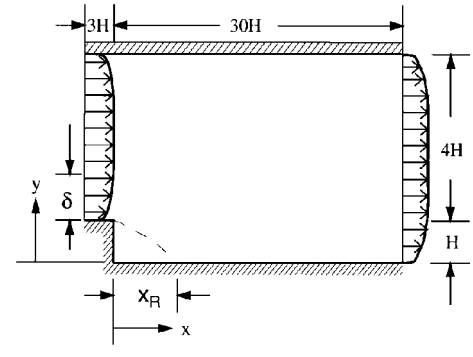

Fig. 17 Geometry of backward-facing step.

is $Re_h = 2.8 \times 10^4$, and the incoming boundary-layer thickness is $\delta/H = 1.1$.

In the present computations, two grids, sizes 78×62 and 150×110, which were nonuniform in both the x and y directions, were used to investigate the effects of grid dependence on the flow predictions. The differences of predictions in the two grids were found to be marginal; therefore in the subsequent computations the 150×110 grid was adopted. The first near-wall grid node was placed at $y^+ \leq 0.3$.

Figure 18 shows the predicted skin-friction coefficient C_f. Launder and Sharma's results were taken from the computations of Heyerichs and Pollard,[21] in which the performances of different model variants were compared and contrasted with measurements. The superior performance of the present model in this complex flow can be further ascertained, in strong contrast to the other two models. One parameter frequently used to examine the performance of the model is the reattachment length. The present prediction indicates that the shear layer reattaches at around $X_R/H = 6.55$, which is close to the measured value, 6.67.

In the present geometry, due to the imposed constant heat flux on the lower wall, a measured Stanton number distribution is also available for comparison. Because steep temperature variation occurs in

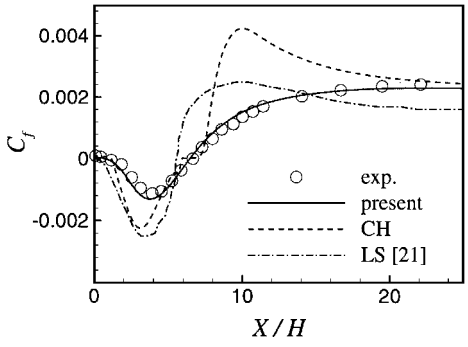

Fig. 18 Predicted skin-friction coefficients.

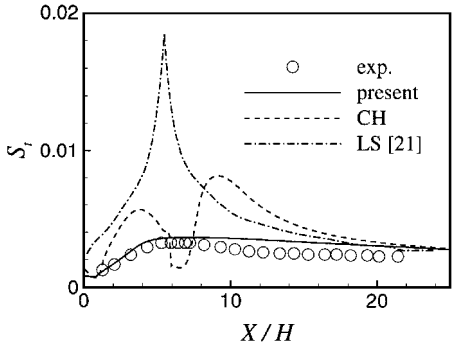

Fig. 19 Predicted Stanton number distributions.

the thin near-wall region, the near-wall turbulence structure influences strongly the wall heat transfer characteristics. Consequently, near-wall turbulence modeling plays an important role in reproducing the correct heat transfer characteristics. The predicted Stanton number distributions are shown in Fig. 19. It has been long recognized that the LS model predicted an excessive heat transfer rate right at reattachment, due to the elevated level of length scale predicted. The common cure of this defect is to damp the growth of the turbulent length scale by the inclusion of the Yap term.[22] The defect of the usage of y^+ in the damping function f_μ can be seen from the CH prediction near the reattachment region. Overall, the present model predicts a correct level of the Stanton number distribution. This is partly due to the correct near-wall dissipation level predicted, resulting from the satisfaction of the asymptotic limit in the vicinity of the wall. The predicted heat transfer performances of the various turbulence models are consistent with the predictions of skin friction. This is expected because it has long been established that for boundary-layer flows N_u is correlated to C_f through the Reynolds analogy.

VI. Conclusion

An improved low-Reynolds-number k–$\tilde{\varepsilon}$ turbulence model is proposed. The model is designed not only to conform with the near-wall characteristics obtained with direct numerical simulation data but also to possess correct asymptotic behaviors in the vicinity of the wall. Key features of the model are the adoption of the Taylor microscale in the damping function and the inclusion of the pressure diffusion terms in both the k and $\tilde{\varepsilon}$ equations to achieve correct limiting behaviors. The performance of the proposed model is first contrasted with the DNS data of the fully developed channel flows. The effect of the inclusion of pressure diffusion terms is reflected by the predicted correct level of ε with the maximum locating at the wall, and in strong contrast, the CH and LS models indicate misplaced local maxima. The performance of the proposed model is further contrasted with the DNS data of the fully developed plane Couette–Poiseuille flow, and the reduction of the k and ε levels at the moving wall side is reproduced correctly by the proposed model. To explore the model's performance in complex environments, the model is further applied to simulate a backward-facing step flow. By contrasting the predicted results with measurements, the results indicate that the present model reproduces correctly the skin-friction coefficients and the near-wall heat transfer behavior.

Acknowledgments

This research was supported by the National Science Council of Taiwan under Grant NSC-85-2212-E-007-023, and the computational facilities were provided by the National Centre for High-Performance Computing of Taiwan, which the authors gratefully acknowledge.

References

[1]Launder, B. E., "Numerical Computation of Convective Heat Transfer in Complex Turbulent Flows: Time to Abandon Wall Functions?," *International Journal of Heat and Mass Transfer*, Vol. 27, No. 9, 1984, pp. 1485–1491.

[2]Jones, W. P., and Launder, B. E., "The Calculation of Low-Reynolds-Number Phenomena with a Two-Equation Model of Turbulence," *International Journal of Heat and Mass Transfer*, Vol. 16, June 1973, pp. 1119–1130.

[3]Launder, B. E., and Sharma, B. I., "Application of the Energy Dissipation Model of Turbulence to the Calculation of Flow Near a Spinning Disc," *Letters in Heat and Mass Transfer*, Vol. 1, No. 2, 1974, pp. 131–138.

[4]Chien, K. Y., "Predictions of Channel and Boundary Layer Flows with a Low-Reynolds-Number Turbulence Model," *AIAA Journal*, Vol. 20, No. 1, 1982, pp. 33–38.

[5]Abe, K., Kondoh, T., and Nagano, Y., "A New Turbulence Model for Predicting Fluid Flow and Heat Transfer in Separating and Reattaching Flows-I. Flow Field Calculations," *International Journal of Heat and Mass Transfer*, Vol. 37, No. 1, 1994, pp. 139–151.

[6]Mansour, N. N., Kim, J., and Moin, P., "Reynolds-Stress and Dissipation Rate Budget in a Turbulent Channel Flow," *Journal of Fluid Mechanics*, Vol. 194, Sept. 1988, pp. 15–44.

[7]Spalart, P. R., "Direct Numerical Simulation of a Turbulent Boundary Layer up to $Re_\theta = 1410$," *Journal of Fluid Mechanics*, Vol. 187, Feb. 1988, pp. 61–98.

[8]Launder, B. E., "Low-Reynolds-Number Turbulence Near Walls," Dept. of Mechanical Engineering, Univ. of Manchester Inst. of Science and Technology, Rept. TFD/86/4, Manchester, England, UK, Feb. 1984.

[9]Kawamura, H., "A k–ε–$\overline{v^2}$ Model with Special Relevance to the Near Wall Turbulence," *Proceeding of the 8th Symposium on Turbulent Shear Flows*, Technical Univ. of Munich, Munich, Germany, 1991, pp. 26.4.1–26.4.6.

[10]Laufer, J., "Investigation of Turbulent Flow in a Two-Dimensional Channel Flow," NACA Rept. 1053, 1951.

[11]Nagano, T., and Tagawa, M., "An Improved k–ε Model for Boundary Layer Flows," *Journal of Fluids Engineering*, Vol. 112, March 1990, pp. 33–39.

[12]Hanjalic, K., and Launder, B. E., "Contribution Towards a Reynolds-Stress Closure for Low-Reynolds-Number Turbulence," *Journal of Fluid Mechanics*, Vol. 74, Pt. 4, 1976, pp. 593–610.

[13]Patel, V. C., Rodi, W., and Scheuerer, G., "Turbulence Models for Near-Wall and Low-Reynolds Number Flows: A Review," *AIAA Journal*, Vol. 23, No. 9, 1985, pp. 1308–1319.

[14]Savil, A. M., "Some Recent Progress in the Turbulence Modelling of By-Pass Transition," *Proceedings of the International Conference on Near-Wall Turbulent Flows*, Arizona State Univ., Tempe, AZ, 1993, pp. 829–848.

[15]Lin, C. A., and Leschziner, M. A., "Three-Dimensional Computation of Transient Interaction Between Radially Injected Jet and Swirling Cross-Flow Using Second-Moment Closure," *Computational Fluid Dynamics Journal*, Vol. 1, No. 4, 1993, pp. 423–432.

[16]Patankar, S. V., *Numerical Heat Transfer and Fluid Flow*, Hemisphere, Washington, DC, 1980, Chap. 6.

[17]Leonard, B. P., "A Stable and Accurate Convective Modelling Procedure Based on Quadratic Upstream Interpolation," *Computer Methods in Applied Mechanics and Engineering*, Vol. 19, June 1979, pp. 59–98.

[18]Rodi, W., and Mansour, N. N., "Low Reynolds Number k–ε Modelling with the Aid of Direct Simulation Data," *Journal of Fluid Mechanics*, Vol. 250, May 1993, pp. 509–529.

[19]Kuroda, A., Kasagi, N., and Hirata, M., "Direct Numerical Simulation of Turbulent Plane Couette-Poiseuille Flows: Effect of Mean Shear on the Near Wall Turbulence Structure," *Proceeding of the 9th Symposium on Turbulent Shear Flows*, Kyoto Univ., Kyoto, Japan, 1993, pp. 8.4.1–8.4.6.

[20]Vogel, J. C., and Eaton, J. K., "Combined Heat Transfer and Fluid Dynamic Measurements Downstream of a Backward-Facing Step," *Journal of Heat Transfer*, Vol. 107, No. 11, 1985, pp. 922–929.

[21]Heyerichs, K., and Pollard, A., "Heat Transfer in Separated and Impinging Turbulent Flows," *International Journal of Heat and Mass Transfer*, Vol. 39, No. 12, 1996, pp. 2385–2400.

[22]Yap, C. R., "Turbulent Heat and Momentum in Recirculating and Impinging Flows," Ph.D. Thesis, Dept. of Mechanical Engineering, Faculty of Technology, Univ. of Manchester, Manchester, England, UK, 1987.

F. W. Chambers
Associate Editor